

---

EFDA-JET-CP(06)02-14

S. Jachmich, T. Eich, W. Fundamenski, A. Kallenbach,  
R. A. Pitt and JET EFDA contributors

# Divertor Particle and Power Deposition Profiles in JET ELMy H-Mode Discharges

“This document is intended for publication in the open literature. It is made available on the understanding that it may not be further circulated and extracts or references may not be published prior to publication of the original when applicable, or without the consent of the Publications Officer, EFDA, Culham Science Centre, Abingdon, Oxon, OX14 3DB, UK.”

“Enquiries about Copyright and reproduction should be addressed to the Publications Officer, EFDA, Culham Science Centre, Abingdon, Oxon, OX14 3DB, UK.”

# Divertor Particle and Power Deposition Profiles in JET ELMy H-Mode Discharges


S. Jachmich<sup>1</sup>, T. Eich<sup>2</sup>, W. Fundamenski<sup>3</sup>, A. Kallenbach<sup>2</sup>,  
R.A. Pitt<sup>4</sup> and JET EFDA contributor\*

<sup>1</sup>Laboratory for Plasmaphysics, Ecole Royale Militaire/Koninklijke Militaire School, EURATOM-Association

<sup>2</sup>Max-Planck-Institut für Plasmaphysik, EURATOM Association, 85748 Garching, Germany

<sup>3</sup>EURATOM/UKAEA Fusion Association, Culham Science Centre, Abingdon, OX14 3DB, UK

<sup>4</sup>Centre de Recherches en Physique des Plasmas, Association EURATOM, Confédération Suisse, EPFL, 1015 Lausanne, Switzerland

\* See annex of J. Pamela et al, "Overview of JET Results",  
(Proc.  IAEA Fusion Energy Conference, Vilamoura, Portugal (2004).

Preprint of Paper to be submitted for publication in Proceedings of the  
17th Plasma Surface Interactions in Fusion Devices,  
(Hefei Anhui, China, 22nd May - 26th May 2006)



## **ABSTRACT.**

The transient pulses of heat and particles arriving at the divertor target plates as a consequence of upstream ELM activity have been characterised at JET using an array of target embedded Langmuir probes in the MarkII SRP divertor. High temporal and spatial resolution of the ELM time behaviour has been achieved by slow divertor strike point sweeps during ELMing H-mode discharges and subsequent coherent averaging of the data. One key result is the observation of target particle flux profile broadening with an e-folding length twice the inter-ELM during Type-I ELMs, presumably as a consequence of the enhanced radial transport. During the ELMs large divertor target currents have been observed, which change sign when the direction of the ion  $B \times \nabla B$  drift is reversed. First comparisons of IR and Langmuir probe derived power deposition profiles have shown a clear increase in the total sheath heat transmission coefficient during the ELMs.

## **1. INTRODUCTION**

The large losses of particles and energy during edge localized modes are a concern for the divertor target plates [1, 2]. For a better understanding of the ELM-physics and for higher confidence in the extrapolation of present day data to ITER, both pedestal ELM-losses and target deposition profile measurements are required. On JET the latter is achieved with a poloidal array of 36 divertor embedded Langmuir probes and a divertor viewing Infra-Red camera. Despite of the comparatively large number of probes the spatial resolution is still poor and often the precise strike point location, where the power and particle fluxes are highest, is often missed by the probe diagnostic. To overcome this problem the inner and outer strike points have been slowly swept over the vertical tiles of the MarkII GB-SRP divertor during the steady-state phase of ELMing H-mode discharges. By measuring the probe currents for different modes of probe operation, ELM and inter-ELM particle flux and temperature profiles are obtained using coherent averaging techniques. This has already been demonstrated as a viable technique, particularly in the sense that the ELMs are sufficiently reproducible for enough data to be available for averaging [3,4]. To study the effect of pedestal collisionality and classical drifts on Type-I and -III ELM fluxes, experiments have been performed with varying heating power, plasma density and magnetic field direction.

## **2. PARTICLE DEPOSITION DURING ELMY DISCHARGES**

The inner and outer strike points were lowered over 4 secs during the flat top phase of a typical Type-I ELMy H-mode discharge with  $B_t = 2.4$  T,  $I_p = 2.0$  MA (giving  $q_{95} = 3.8$ ), auxiliary neutral beam heating of 13 MW and in forward and reversed  $B_t$ , where by forward field is meant the ion  $B \times \nabla B$  drift direction downwards. Table 1 compiles a number of key parameters in these discharges. When  $B_t$  has been reversed also  $I_p$  has been reversed to keep the helicity. Recycling emission in the inner and outer divertor indicates that the strike point sweep had only a marginal effect on the ELM-behaviour. The ELM-frequency of 50 Hz and the ELM-size remain almost constant, allowing the application of coherent averaging techniques. Each discharge was repeated three times with the probes being biased

either negatively in ion saturation potential  $V_{pr} = -100$  V, at  $V_{pr} = 0$  to obtain the current at zero volts and at positive potential  $V_{pr} = +20$  V giving three operating points on the coherent Langmuir probe characteristic and allowing the determination of electron temperature. A complete divertor profile was constructed from the profiles individually measured by the probes, whereby at the outer divertor typically eight probes have been used. In regions, where the individual profiles overlap, the data agreed very well, which is an important requirement for the application of the coherent averaging technique. Figure 1 shows the particle flux profile during Type I ELMs for the case of forward field. The times indicated are relative to the time, when the ion saturation current of the probe closest to the strike point reaches its maximum. The profile for  $t=0$  is further on referred to as ELM-profile. The data are further normalized to the maximum of the profile and all radial positions are mapped to the outer midplane. From the logarithmic scale it is very evident that the deposition profile remains exponential during the ELM. The decay length obtained from a least square fit is roughly twice as large as the inter-ELM value. Such broadening has not been observed in the total power deposition as measured by the JET divertor viewing Infrared-cameras [5]. Though heat fluxes are the main concern from the point of view of divertor lifetime, the particle profile is a reasonable indication for the power deposition, since the ion saturation current increases fairly linearly with the power released by the ELM for the range of 50–200 MW, in which the discharges presented here lie [6]. Whether the difference in broadening seen by the IR compared with the LP is brought about by the sheath transmission factor or by the electron temperature profile, is presently beyond our judgment.

Interestingly, Figure 2 shows that although reversing the magnetic field and plasma current direction, causes the inter-ELM particle flux profile to broaden, it has no effect on the ELM-profile itself. Nevertheless, both profiles for the forward and reversed B case at the time of the ion saturation current maximum have similar large decay lengths. This observation is an indication for the curvature-driven mechanism of the Type-I ELMs, which leads to an enhanced radial transport during the ELM [7]. On the contrary this seems not to be the case for the Type III ELMs, where reversing B has a substantial effect on Type III ELMs. During the ELM the inter-ELM profile shape is preserved, i.e.  $\lambda$  does not change. Finally, we like to point to a further proof of the reliability of coherent averaging seen in figure 2. The shape of the inter-ELM forward B profile is clearly double exponential, which has also been previously reported for non-averaged data [8].

### 3. TARGET CURRENTS DURING ELMs

By fixing the probe bias potential at zero volts (i.e. at target potential), the current flowing between the targets and the plasma can be measured on a fast timescale. Using the coherent averaging technique reveals large changes in the target currents during ELMs. Figure 3 shows profiles of  $J_0$  at the inner and outer target during Type I ELMs for both forward and reversed field. Positive currents are net ion currents flowing into the divertor corresponding to the ion diamagnetic drift direction in forward B. The inter-ELM profiles ( $t = -0.3$  ms) are in good agreement with earlier observations in ohmic discharges [9]. In reversed B, the currents at the inner divertor change sign. At the outer divertor this is not

obvious, though the radially integrated profile tends to be in the same direction as at the inner. During the ELM the current distribution of the inner and outer target is very asymmetric and net currents up to 25kA in forward B and  $-20$  kA in reversed B are lost to the divertor. Similar observations in sign and amplitude have also been made for Type III ELMs. By associating the pedestal temperature with the current carrying particle flux, we find for the energy integrated over the ELM,  $E_{j_0} = \int \int \frac{3}{2} k T_e |j_{0,net}/e| dA$ , 46kJ and 52kJ respectively for the forward and reversed B-field case.

#### 4. POWER DEPOSITION AND SHEATH ENERGY TRANSMISSION FACTOR

Theoretical models (fluid and kinetic) indicate that the ELM transient provokes considerable variations in the sheath heat transmission factors at divertor targets [10–12]. Providing experimental confirmation of this is a key element towards building confidence in these models and improving their predictive capability for ELM fluxes to be expected in ITER. The sheath energy transmission factor, which is measure of the energy per ion-electron pair transmitted across the sheath is defined as  $\gamma = Q_{tot}/kT_e\Gamma_{||}$  GP [13], and can be written as the sum of sheath transmission factors for the ions  $\gamma_i$  and for the electrons  $\gamma_e$ . Sheath theory predicts

$$\gamma \approx 2.5 \frac{T_i}{T_e} + \frac{2}{1 - \delta_{see}} - 0.5 \ln \left( 2\pi \frac{m_e}{m_i} \left( 1 + \frac{T_i}{T_e} \right) / (1 - \delta_{see})^3 \right) \quad ; \quad (1)$$

for isothermal plasmas with  $T_i = T_e$  and without any secondary electron emission one expects  $\gamma \sim 7.3$ . Assuming a secondary electron emission  $\delta = 0.55$  for the JET-divertor probes [14], a value of 9.0 is obtained for  $\gamma$ .

From dedicated measurements of  $g$  in tokamaks energy transmission factors ranging from 6 up to 100 in steady state have been reported in the past [15–17], leading to large uncertainties in the determination of the power load. To the authors' knowledge, no attempt has yet been reported to measure gamma during the ELM transient itself.

This has been attempted at JET using a dedicated discharge and combining IR camera derived target heat fluxes with Langmuir probe measurements. In this case the coherent ELM technique is less appropriate since both particle flux and  $T_e$  are required on a fast timescale and insufficient reproducible discharges were available to provide matched pulses in which the probe operation mode could be varied from pulse to pulse. Instead, the strike points were fixed and positioned so as to optimise the IR spatial resolution and be located on the inner a target close to a pair of triple probes still in operation at the time of the experiment. Attributing the IR measured power  $Q_{IR}$ , to the sum of the ion and electron powers flowing onto the surface of the tile,  $g$  can be obtained as

$$\gamma = \frac{Q_{IR}}{kT_e J_{i,sat} \sin \alpha} \quad (2)$$

where  $\alpha$  as the magnetic field line angle with respect to the tile surface. The discharge parameters are

listed in table 1. Fast diamagnetic measurements show that during an ELM about 12% of the pedestal energy is lost, which corresponds to a release of 190kJ into the SOL. Integrating the ELM deposited IR power over time and tile surface yields 120kJ at the inner divertor and 52kJ at the outer. To improve statistics the ELM signals have again been coherently averaged using the vertical Da-signal. Figure 4a shows the IR ELM power together with that measured by the LP using the conventional assumption of  $\gamma = 8$  at a position 2.8cm above the inner target strike point. The time  $t=0$  is defined to be the maximum of the Da ELM peak and does not necessarily represent the time, when the ELM is triggered at the outer midplane. The error-bar on QIR results from the uncertainty in the heat transmission coefficient due to the presence of surface layers on the inner tile [5]. Three different values for the parameter, which simulates the effect of the surface layer have been tried. For the further analysis the mean value of the three calculated QIR has been used. The error-bar on the LPmeasurements uses an instrumental error of 10% on the voltage and current measurements, together with 20% uncertainty on the effective probe projected area due to erosion.

The time evolution of the sheath transmission factor at two different locations one in the SOL (strike point distance  $d=2.8\text{cm}$ ) and one in the PFR ( $d=-1.4\text{cm}$ ) using the above measurements are shown in fig.4b. At the time of the  $D_\alpha$ -peak, very high values of the sheath transmission factor are derived. Independently of any theoretical interpretation, the fact that the IR power peaks well in advance of the LP power leads to the expectation that gamma should be high at the beginning of the transient. The large values of  $\gamma$  could be caused by fast electrons, which are not repelled by the probes, or hot ions arriving at the target. Also enhanced secondary electron emission, which might occur in JET due to the warming-up of the target surfaces during an ELM, could also lead to high  $g$ . Towards the end of the ELMBurst the gamma measured in this way increases again, since the IR still sees power arriving at the target, whereas the LP do not. In between ELMs the probe data indicate that the inner divertor tends to detach with  $T_e \sim 5\text{eV}$  at the measurement position. The time average of  $g$  during the ELM has a value of 11. Similar results have been obtained from Particle-in-Cellsimulations [10], albeit for different discharge parameters. Here  $g$  reaches 38, which is due to the enhancement of  $g_e$  shortly after the ELM. This leads to two maxima in the time trace of  $\gamma$ , which is also seen in Fig.4b and has recently been predicted in [12] by kinetic modelling. The time traces, shown in Fig.4c, are derived from a parameterized expression for  $\gamma_i$  and  $\gamma_e$  as given in [12] using the pedestal parameters of the discharge ( $\tau_{\parallel,i} \sim 250\mu\text{s}$ ,  $\tau_{\parallel,e} \sim 8\mu\text{s}$ ,  $C_e = 100$ ,  $C_i = 30$ ). Despite the various uncertainties which plague the use of IR and LPs for power flux measurements, the predicted time response during the transient reproduces remarkably well the experimentally observed temporal behaviour.

## CONCLUSIONS

It has been demonstrated, that despite of the stochastic nature which is inherent in ELMs, reliable profiles particle, heat and current flows onto to the target can be reconstructed from Langmuir probe data. Large decay lengths in the SOL during Type-I ELMy discharges have been found, which also exist when  $\mathbf{B} \cdot \hat{\mathbf{N}}$  is pointing away from the X-point. The ELMevents are accompanied by large



currents flowing onto the targets. Again reversing the B-field changes the in/out asymmetry and the currents reverse sign. For both cases the current balance of the inner and outer divertor shows net currents lost during the ELM in the order of 1% of the plasma current.

The large sheath transmission factor, which appear instantaneously at the ELM-event, have been predicted by kinetic modelling and confirm that any simple fluid picture is not applicable to ELMs. The consequence of this result is also that one cannot directly conclude from measured electron heat fluxes, the total power arriving at the target. Being aware of the difficulties, which the IR- and LP-diagnostics have in the data interpretation, the measurement of the divertor power load remains still a challenge.

#### **REFERENCES:**

- [1]. D.J. Campbell, Phys. Plasmas **8** (2001) 2041.
- [2]. G. Federici, Plasma Phys. Control. Fus. **45** (2003) 1523.
- [3]. M. Laux et al., Proc. 28th EPS Conf. on Contr. Fus. and Plasm. Phys. 25A (2001) 1625.
- [4]. R. Pitts et al., Nucl. Fusion **43** (2003) 1145.
- [5]. Th. Eich et al., J. Nucl. Mat. **337-339** (2005) 669.
- [6]. J. Lingertat et al., J. Nucl. Mat. **241** (1997) 402.
- [7]. W. Fundamenski et al., Plasm.Phys. Contr. Fus. **46** (2004) 233.
- [8]. W. Fundamenski et al., Plasm.Phys. Contr. Fus. **44** (2002) 761.
- [9]. M.J. Schaffer et al., Nucl. Fus. **37** (1997) 23.
- [10]. D. Tskhakaya et al, Theory of Fusion Plasmas ed J.W. Connor et al (2004) Societa Italiana di Fisica, Bologna, Italy.
- [11]. A. Bergmann et al., Nucl. Fusion **42** (2002) 1162.
- [12]. W. Fundamenski, R.A. Pitts et al., Plasm.Phys. Contr. Fus. **48** (2006) 109.
- [13]. R.C. Bissell, P.C. Johnson and P.C. Stangeby, Phys. Fluids B **1** (1989) 1133.
- [14]. E.W. Thomas, Supp. Nucl. Fusion **1** (1991) 79.
- [15]. R. Budny, D. Manos, J. Nucl. Mat. **121** (1984) 41.
- [16]. K. Ertl, J. Nucl. Mat. 128&129 (1984) 163.
- [17]. P.K. Mioduszewski, P.H. Edmonds, L.H. Emerson, J. Nucl. Mat. 145&147 (1987) 210.

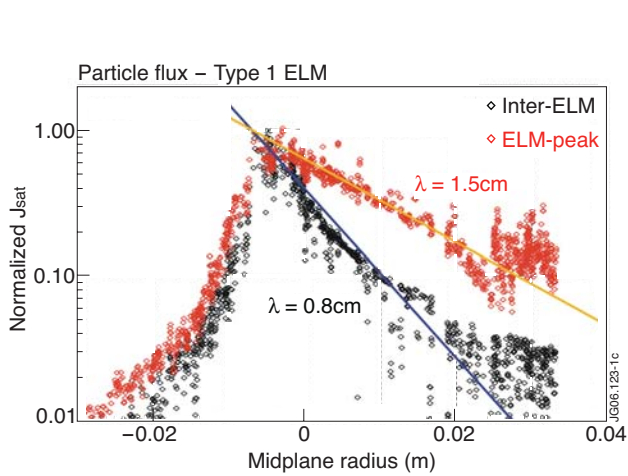


Figure 1: Profiles of particle flux to the outer divertor during Type I ELMs (red) and in between ELMs (black).

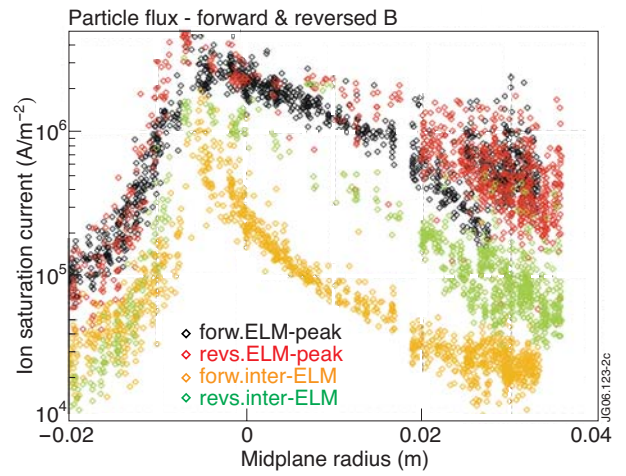


Figure 2: Profiles of  $J_{sat}$  to the outer divertor at the peak of Type I ELMs (black, red) and of the inter-ELM level (yellow, green) respectively for the forward and reversed B-field discharges.

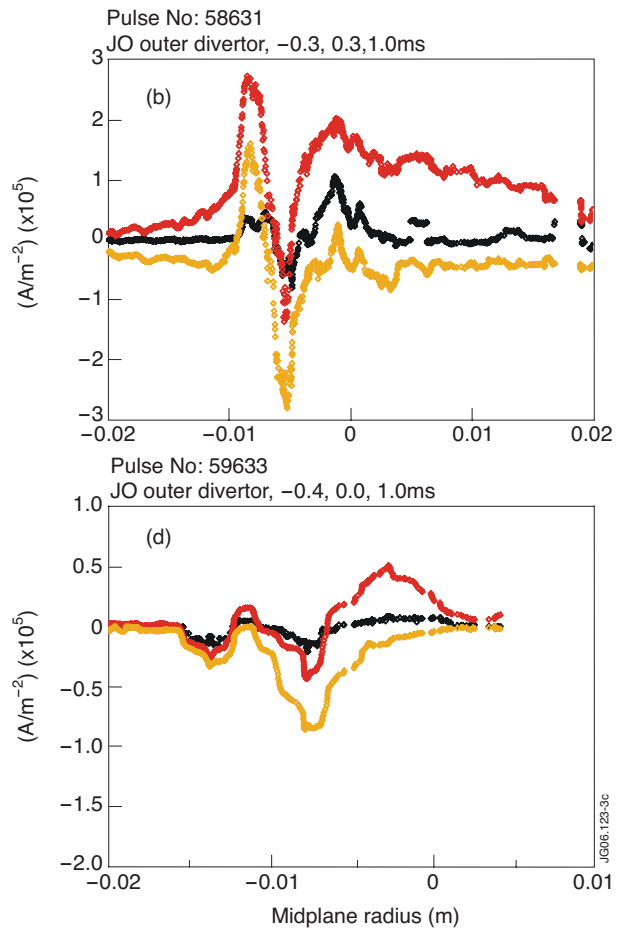
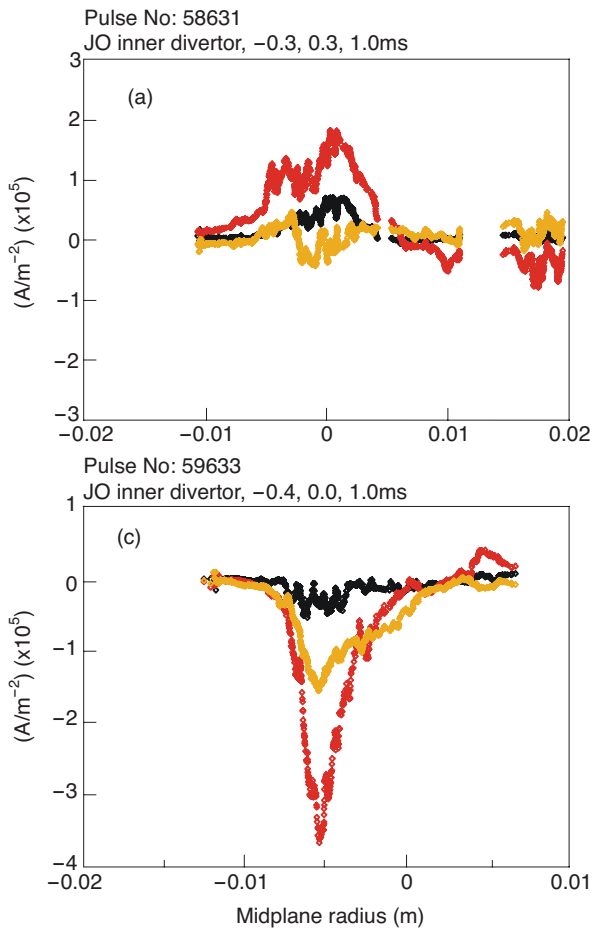


Figure 3: Target currents arriving at the inner (left column) and outer divertor during Type I ELMs in forward-B (a&b) and reversed-B (c&d) discharges (black = -0.3ms, red = 0.3ms, yellow = 1.0ms).

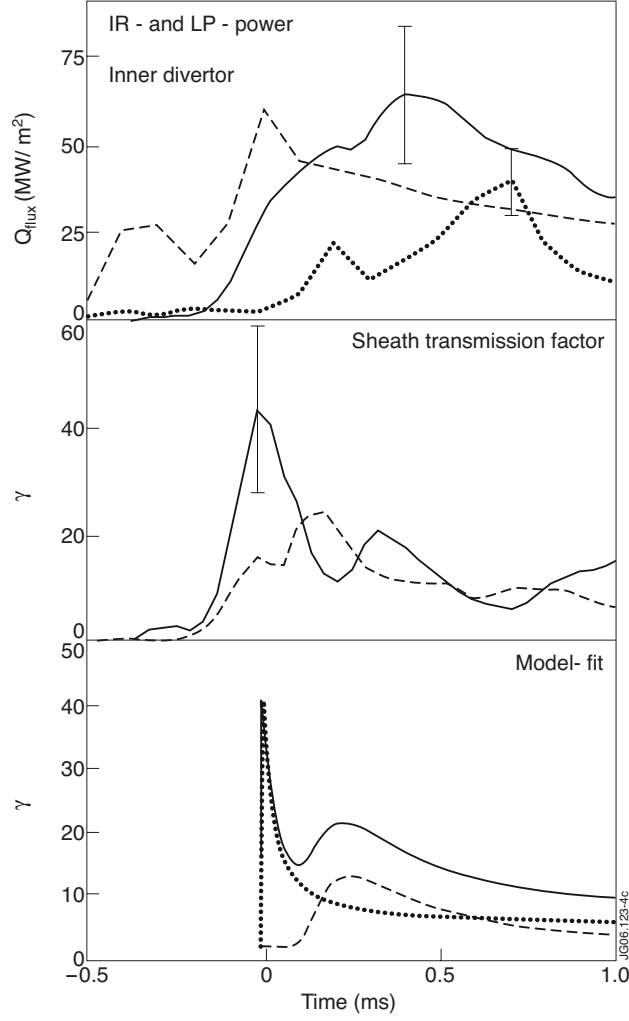


Figure 4: Time evolution of (a) heat fluxes measured by IR (solid) and LP using  $\gamma=8$  (dashed) at a position 2.8cm away from the strike point and of the divertor recycling  $D_\alpha$  used for the averaging (dotted). (b) Sheath transmission factor for the same position as in (a) (solid) and in the PFR ( $d = -1.4$  cm, dashed). (c) Modeled total (solid), electron (dashed) and ion (dotted) sheath transmission factor.

	ELM	$B_t/T$	$I_p/MA$	$P_{NBI}/MW$	$q_{95}$	$f_{ELM}/HZ$	$n_{ped}/10^{19} m^{-3}$	$T_{e,ped}/eV$	$\nu^*$
forward B/ low gas	I	-2.4	-2.0	13.1	3.8	~50	~4.2	~800	0.34
forward B/ high gas	III	-2.4	-2.0	13.1	3.8	~95	~5.0	~400	0.72
reversed B/ low gas	I	+2.4	+2.0	12.7	3.9	~42	~4.0	~600	0.57
reversed B/ high gas	III	+2.4	+2.0	13.0	4.0	~170	~3.5	~400	1.1
pulse, $\gamma$ determined	I	-2.4	-2.0	12.0	3.8	22	~3.4	~1200	0.11

Table 1: Main parameter of the reference discharges.